Waterjet Propulsion and Negative Thrust Deduction

Fourth International Symposium on Marine Propulsors
smp'15, Austin, Texas, USA, June 2015

Waterjet Propulsion and Negative Thrust Deduction

Arash Eslamdoost, Lars Larsson, Rickard Bensow

Department of Shipping and Marine Technology,
Chalmers University of Technology, 412 96 Gothenburg, Sweden

ABSTRACT

The thrust deduction fraction of waterjet-propelled hulls is often reported to be negative in the speed range close to the operating speeds. In this paper, employing a numerical method, the bare hull and the self-propelled hull flows are studied. The changes between the bare hull and self-propelled hull resistances are investigated for understanding whether it is the waterjet hull resistance decrease which contributes to the negative thrust deduction fraction or there are some other effects rather than the resistance increment.

Keywords

Waterjet propulsion, Thrust deduction fraction, Resistance increment, Intake drag, Exit drag, CFD.

1 INTRODUCTION

The thrust deduction fraction indicates the relation between the bare hull resistance and the thrust required to propel a vessel. In case the vessel is propelled by means of a propeller, the net thrust of the propeller is employed to define the thrust deduction fraction as follows,

$$t = 1 - \frac{R_{bh} - R_a}{T_{net}}, \qquad (1)$$

where R_{bh} and T_{net} are the bare hull resistance and the net thrust of the propeller. R_a is called rope force and is applied to the self-propelled model to unload the extra frictional resistance of the model comparing to the full scale ship.

The net thrust of a propeller is transmitted through its shaft to the hull and it is rather an easy task to measure this force, which is not the case for a waterjet unit. In contrast to a propeller, there is more than just a single contact point between the hull and the waterjet unit which makes it tricky to measure the net thrust of the waterjet unit. In the early days of waterjet testing at MARIN it was tried to directly measure the net thrust of the waterjet unit by isolating the entire unit from the hull including the driving motor on a force measuring frame and seal the gaps between the hull and the waterjet unit to avoid leakage. Complications of this method such as the adverse dynamic mass-spring characteristics of the measuring frame and the costs involved put an end to further development of this measurement technique (van Terwisga 1996). In order to skip the impracticality of the measurement of the waterjet unit net thrust, the ITTC High Speed Vehicle Committee (ITTC 1987) suggested to use gross thrust, T_g, which is the momentum flux change through the waterjet control volume defined in Figure 1.

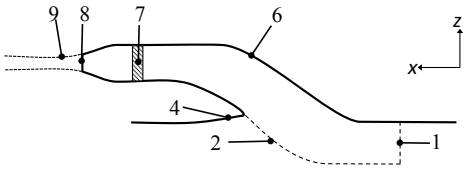

Figure 1 Section cut through the waterjet ducting system

Figure 1 shows the cross section of a waterjet propulsion unit and the control volume, which is mostly applied for the system analysis. Surface 2 is a streamtube, which separates the flow drawn into the ducting system from the rest of the flow field and surface 1 is the cross section of the streamtube "far enough in front of the intake ramp tangency point, before inlet losses occur" (ITTC, 1996) and as a practical solution, the ITTC Specialist Committee on the Validation of Waterjet Test Procedures recommends one inlet length forward of the ramp tangency point (ITTC, 2005). Surface 6 is the waterjet system internal material boundaries that extend to the capture area; Surface 7 is the boundary area of the pump control volume and surface 8 represents the nozzle discharge area. The jet vena-contracta, where the jet cross-section mean static pressure equals the atmospheric pressure, is shown with surface 9. The jet cross sectional area is minimum at the vena-contracta.

The gross thrust, $\vec{T}_g$, as defined by van Terwisga is "the force vector pertinent to the change in momentum flux over the selected control volume, acting on its environment" (van Terwisga 1996). For the sake of simplicity, in the rest of this paper the term gross thrust refers to the horizontal component of the gross thrust vector, which is of interest. Writing the horizontal momentum flux balance over the control volume shown in Figure 1 yields,

$$T_g = -\iint_{A_1+A_8} \rho u_x (u_k n_k) dA, \quad (2)$$

where ρ is the density of the fluid, u is the velocity vector and n is the unit vector normal to the control surface pointing outward of the control volume. The Einstein notation is used in Equation (2) where index k ranges over 1, 2 and 3.

The total thrust deduction fraction of a waterjet propelled craft, then can be based on the gross thrust as follows,

$$t = 1 - \frac{R_{bh} - R_a}{T_g}. \quad (3)$$

Figure 2 shows a collection of thrust deduction fraction for different hulls. The overall trend of this collection shows that t has large positive values in the low speed ranges and has small negative values in the intermediate speed range and then approaches small positive values in the higher speed range. The focus of this paper is to investigate the reasons for negative thrust deduction fractions in the intermediate speed range. In order to be able to proceed with this investigation some more definitions are explained in the following.

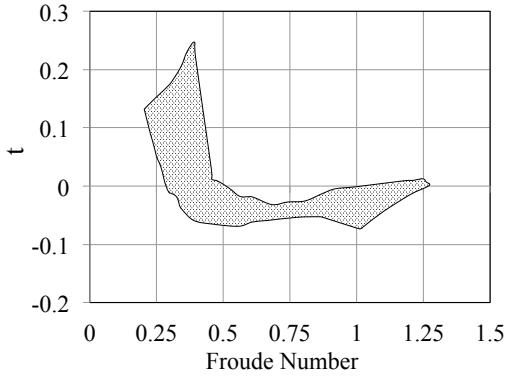

Figure 2 Collected thrust deduction fraction (van Terwisga 1996)

Considering the material boundaries of the waterjet system, "the net thrust, $\vec{T}_{net}$, is defined as the force vector acting upon the material boundaries of the waterjet system, directly passing the force through to the hull" (van Terwisga 1996). Like the gross thrust gross thrust in this paper, the horizontal component of the net thrust vector will be called net thrust, T_{net}, and is defined as,

$$T_{net} = -\iint_{A_4+A_6} \sigma_x dA - \iiint_{V_7} \rho F_{px} dV, \quad (4)$$

where σ_x is the x-component of the surface stresses (pressure and shear stresses) and F_{px} is the x-component of the pump force distribution per unit mass.

As mentioned earlier, it is a tricky task to measure the net thrust of a waterjet unit but with the aid of CFD it is possible to obtain the terms shown in Equation (4). Then the hull resistance increment fraction based on the net thrust of the waterjet unit would be as follows,

$$t_r = 1 - \frac{R_{bh} - R_a}{T_{net}}. \quad (5)$$

The gap between the total thrust deduction fraction and the resistance increment fraction is the jet system thrust deduction fraction, t_j, plus a second order term including t_r and t_j, as follows (Eslamdoost 2014),

$$t = t_r + t_j - t_r t_j. \quad (6)$$

The jet system thrust deduction fraction formulation and its computation method are discussed in Section 5.3.

The question is whether the negative thrust deduction fraction in the intermediate speed range ($0.5 < Fn < 1.0$) is due to a resistance reduction in self-propulsion (t_r negative), or due to a smaller gross thrust than net thrust ($t_j - t_r t_j$ negative). Van Terwisga (1996) states that the net and gross thrusts are almost the same in this speed range, while Bulten (2006) concludes that the net and gross thrusts are significantly different. The present authors argue in (Eslamdoost et al. 2014a) that there is little reason for a reduction in resistance in self-propulsion, i.e. t_r should be close to zero. The negative thrust deduction must then be due to t_j. In the present paper the different contributions to t_r and t_j are quantified for a high-speed hull with $t = -0.09$ at $Fn = 0.8$. The relative importance of t_r and t_j is discussed and a conclusion is drawn on the reason for the negative thrust deduction.

2 METHOD

The hull used in the study is a planing mono-hull with a single waterjet unit. Employing the code STAR-CCM+, a Finite Volume method in combination with control volumes consisting in a predominantly hexahedral mesh is used to solve the unsteady mass and momentum conservation equations in integral form. The Volume of Fluid (VOF) method is used to trace the free surface. The realizable k- ε turbulence model with wall functions is used to solve the turbulence effect on the mean flow. The sinkage and trim of the hulls are fixed to the measured values obtained from resistance and self-propulsion tests carried out at SSPA (Brown 2013). For modeling the waterjet unit the actual geometry of the ducting channel including the shaft and the hub is employed in the numerical simulation but instead of modeling the actual rotating impeller and the stator geometry an axial body force equal to the resistance of the entire hull/waterjet system is uniformly distributed inside the compartment containing the impeller. This body force acts as a momentum source and accelerates the flow in the axial direction.

3 HULL AND PUMP GEOMETRY

The hull geometry used in this study is a test case designed at SSPA. For the self-propulsion test the hull was equipped with a single waterjet propulsion unit designed by Rolls-Royce. The hull geometry and the positioning of the waterjet unit on the hull are shown in Figure 3. During the resistance and self-propulsion tests the waterjet unit was mounted on the hull throughout both the resistance and self-propulsion test, but during the resistance test the intake opening was covered and the unit was filled with water to create the same initial conditions for the bare hull and self-propelled one.

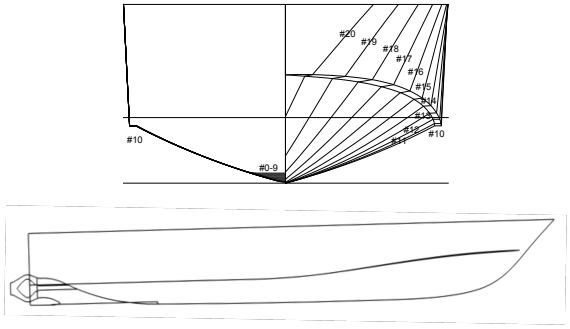

Figure 3 Hull geometry and positioning of the waterjet unit.

4 MESH GENERATION AND VERIFICATION

For consistency between the bare hull simulations and the ones for the waterjet driven hull it is tried to keep the grid generation technique as well as the mesh size and mesh distribution the same as for the bare hull. However, the geometries are not exactly the same and a larger number of cells is required for the self-propulsion computational domain to generate the grid inside the waterjet unit. The grid distribution in the computational domain is shown in Figure 4 and Figure 5. Since the flow details into the waterjet intake and the discharged flow out of the nozzle are of interest, the mesh in these regions is refined further.

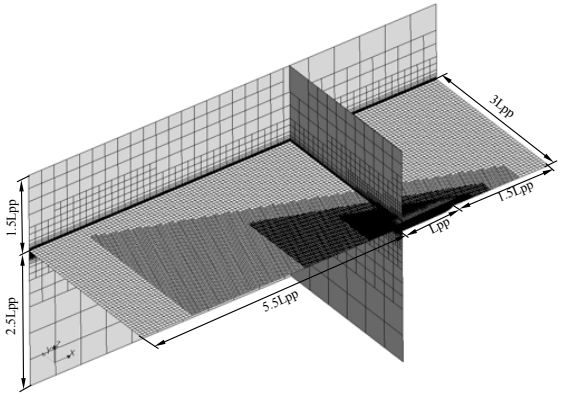

Figure 4 Grid distribution in the computational domain.

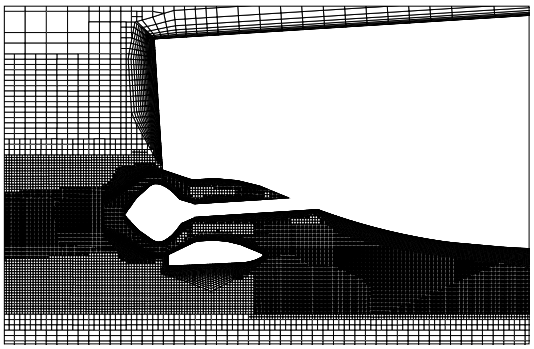

Figure 5 Grid distribution inside the ducting channel.

To obtain a suitable cell size, and hence total grid number, a systematic grid refinement study was carried out for the bare hull and self-propelled hull grids. Multiple grids with systematically varied grid parameters were used at Froude number 0.798 for the waterjet-driven hull. The mesh convergence study was carried out by studying the resistance coefficient of the hull which is defined as follows,

$$C_T = \frac{R_T}{\frac{1}{2}\rho S_{ref} U^2}, \tag{7}$$

where R_T is the total resistance of the hull, ρ is the water density, S_{ref} represents the wetted surface of the hull at rest and U is the ship velocity.

The total resistance coefficient convergence curve for the self-propelled hull is plotted in Figure 6. Since the grid is unstructured the step size h_i on the horizontal axis is obtained as the third root of the total number of cells for grid i. The finest grid is denoted by h_1. The total number of cells for this grid is $16.2E6$ and for the coarsest grid it is $1.2E6$.

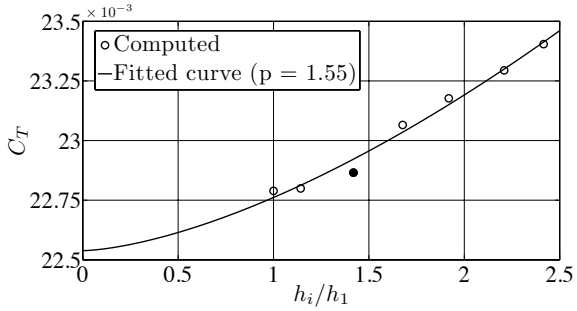

Figure 6 Convergence of the total resistance coefficient with grid refinement at $Fn = 0.798$ for the waterjet driven hull. The full symbol show the grid employed to perform the calculation for the entire range of Froude numbers. The p-value is the power of the best fit expression for the error according to Eça and Hoekstra (2014).

The formal verification which is carried out based on the Least Squares Root method by Eça and Hoekstra (2014)

indicates that a good compromise between numerical accuracy and computational effort is obtained with the grids shown by the full symbol in Figure 5, which is selected for further self-propulsion computations. The total number of cells for this grid is $5.7E6$. The numerical uncertainty for this grid is 2.3% of the computed resistance coefficient.

5 RESULTS AND DISCUSSION

An overall view of the pressure distribution inside the ducting channel as well as the free-surface behind the waterjet-propelled hull are shown in Figure 7 and Figure 8, respectively.

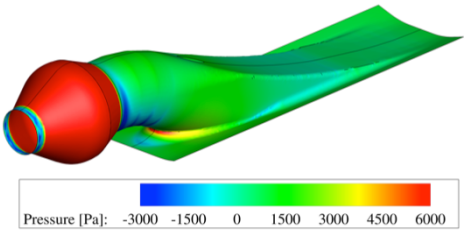

Figure 7 Pressure contour inside the ducting channel at Fn = 0.8.

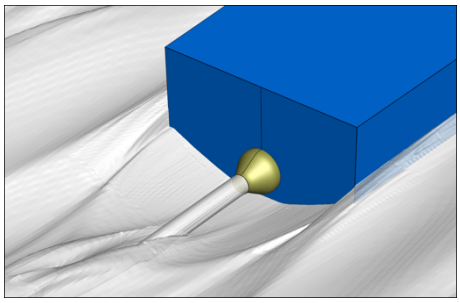

Figure 8 Simulated free-surface and jet flow at Fn = 0.8.

The validation of the computed quantities (e.g. bare hull resistance, gross thrust, thrust deduction fraction, …) can be found in Eslamdoost et al. (2014b) and Eslamdoost (2014). The computed thrust deduction fraction at Froude number 0.8 is -0.09. In the following sections the reasons for the negative thrust deduction fraction are explained by studying the hull resistance increment fraction and the jet system thrust deduction fraction (the terms which appear in Equation (6)).

5.1 Resistance Increment

The resistance increment of the hull is studied in this section. In order to understand whether it is the sinkage/trim changes or the local flow change due to the waterjet action which contributes to the resistance increment, a third hull (other than the bare hull (BH) and the self-propelled hull (SP)) is introduced. This hull is a bare hull that has the same sinkage and trim as the waterjet-driven hull (BH_{SP}). Comparison of the resistance change between BH_{SP} and BH identifies the effect of the global flow change on the resistance increment and the comparison between SP and BH_{SP} identifies the effect of the local flow on the resistance increment. The total effect is obtained by comparing SP and BH directly. Each of the global, local and total effects are studied through splitting the components of the resistance in two levels. The first level is to split the total resistance into the resistance of the transom and the resistance of the rest of the hull, which in the following discussion is mentioned as 'hull'. Then at the second level the resistance of the hull and the transom individually are split into pressure and frictional resistance, where the pressure resistance in turn is split into hydrostatic and hydrodynamic resistance.

The computed thrust deduction fraction and the resistance increment fraction at $Fn = 0.8$ are -0.09 and -0.01, respectively. The speed in this range is beyond the critical Froude numbers for transom clearance, so there is no hydrostatic or hydrodynamic force acting on the transom and it is the change of forces acting on the hull that contribute to the resistance increment. The resistance increment components due to the global, local and total effects are presented in Table 1 and schematically in Figure 9. In the following, the resistance increment components of the hull are analyzed by investigating the changes of the resistance components between the bare hull and the self-propelled hull.

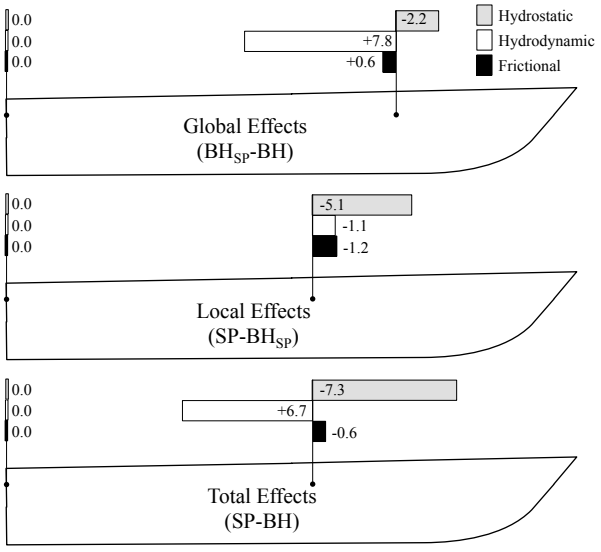

Figure 9 Schematic presentation of the hull and the transom resistance increment components at $Fn = 0.80$. Bars represent force changes in Newton. Positive changes backwards. The bare hull resistance at this speed is $110.4\ N$.

Table 1 Resistance components of hulls $Fn = 0.80$.

		Components			Increments		
		SP	BH	BH_{SP}	SP-BH	BH_{SP} -BH	SP- BH_{SP}
Transom	Hydrostatic	0	0	0	0	0	0
	Hydrodynamic	0	0	0	0	0	0
	Friction	0	0	0	0	0	0
	Total	0	0	0	0	0	0
Hull	Hydrostatic	+18.0	+25.3	+23.1	-7.3	-2.2	-5.1
	Hydrodynamic	+63.8	+57.1	+64.9	+6.7	+7.8	-1.1
	Friction	+27.4	+28.0	+28.6	-0.6	+0.6	-1.2
	Total	+109.2	+110.4	+116.6	+1.7	+6.2	-7.4
Total Resistance	Hydrostatic	+18.0	+25.3	+23.1	-7.3	-2.2	-5.1
	Hydrodynamic	+63.8	+57.1	+64.9	+6.7	+7.8	-1.1
	Friction	+27.4	+28.0	+28.6	-0.6	+0.6	-1.2
	Total	+109.2	+110.4	+116.6	-1.2	+6.2	-7.4
				$100\times(\Delta R)/R_{ref}$	-1.1%	+5.3%	-6.3%
				$t_r = \Delta R/R_{final}$	-0.01	+0.06	-0.07

Comparing the self-propelled hull resistance with that of the bare hull, it is seen that the total resistance of the hull changes by $-7.3\,N$ due to the change in the hydrostatic resistance of the hull. The global effect contribution to the hydrostatic pressure resistance increment of the hull is $-2.2\,N$. Although BH_{SP} sinks deeper compared to BH ($6\,mm$ at mid-ship[1]) its smaller trim angle ($0.2°$ less) positions the hull such that the hydrostatic pressure on the fore part cancels to a larger extent the hydrostatic pressure on the aft part of the hull. This is the reason for the reduced hydrostatic pressure resistance due to the global effects. The local effects also cause a reduction ($-5.1\,N$) in the hydrostatic pressure resistance of the hull. The major part of this reduction ($-4.9\,N$) is caused by the missing intake opening area. At Froude number 0.8, the trim angle of the hull ($\sim 3.8°$) positions the intake-opening surface such that the hydrostatic force acting on this surface has an axial component pointing backward. Removing this surface will result in a decreased hydrostatic resistance of SP. The rest of the hydrostatic pressure resistance increment due to the local effect ($-0.2\,N$) is caused by the intake-induced flow, which alters the waves close to the aft part of the hull.

The hydrodynamic pressure resistance of SP is $+6.7\,N$ larger than that of BH. The hydrodynamic pressure resistance increment due to the global effects is $+7.8\,N$. The local effects contribution to the hydrodynamic pressure resistance increment works in the opposite direction and changes the resistance by $-1.1\,N$. The reason for the resistance increase due to the global effects is the deeper sinkage ($6\,mm$ at mid-ship), which gives an increased displacement and thereby a higher hydrodynamic pressure on the bottom (Figure 11). The reason for the resistance reduction due to the local effects is the missing intake surface. As stated in the discussion of the hydrostatic pressure resistance of the hull, the intake-opening surface is inclined such that its normal vector has a component which points to the forward direction.

Comparing BH_{SP} and BH, it is seen that the increased sinkage and decreased trim angle result in increased wetted surface area of the hull and therefore the frictional resistance of BH_{SP} increases ($+0.6\,N$) but comparing SP and BH_{SP} the frictional resistance is seen to decrease due to the missing surface of the intake-opening ($-1.2\,N$). The result of these two effects is a frictional resistance change of $-0.6\,N$.

At this operating Froude number, the hull hydrostatic, hydrodynamic and frictional resistances vary such that the sum of all these variations becomes almost zero, and that is the reason for obtaining almost zero resistance increment fraction in the intermediate operating speed range.

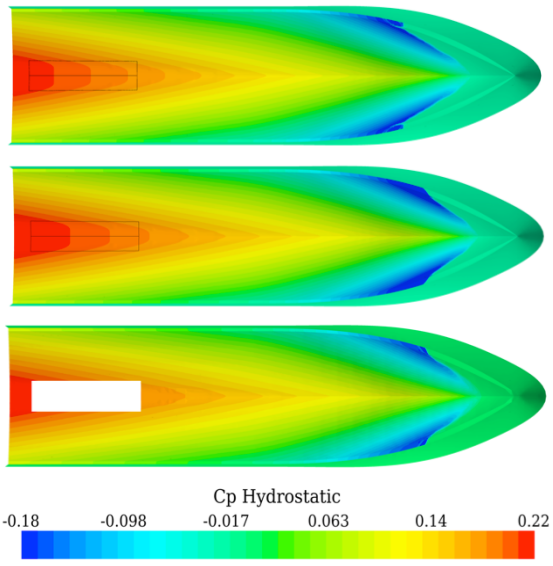

Figure 10 Hydrostatic pressure coefficient contour on BH (top), BH_{SP} (middle) and SP (bottom) at $Fn = 0.8$. The bold black line shows the intake-opening region.

[1] The bare hull moves upwards by almost $25\,mm$ at mid-ship at $Fn = 0.8$.

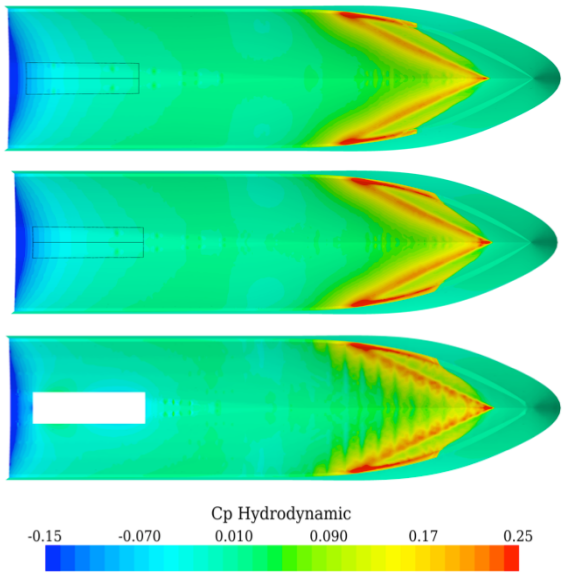

Figure 11 Hydrodynamic pressure coefficient contour on BH (top), BH_{SP} (middle) and SP (bottom) at $Fn = 0.8$. The bold black line shows the intake-opening region.

5.2 Net Thrust and Gross Thrust Relation

In his doctoral thesis, Eslamdoost (2014) shows that the net thrust (resistance of the self-propelled hull) defines the trend of the thrust deduction fraction and that the gross thrust, to a large extent, follows the trend given by the resistance changes of the self-propelled hull. The difference between the gross thrust and the net thrust is the sum of the intake and the exit drag,

$$T_g - T_{net} = -\iint_{A_1+A_2+A_8} \sigma_x dA + \iint_{A_4} \sigma_x dA = D_i + D_e. \qquad (8)$$

The intake drag, D_i, is the resultant of the forces acting on the capture area (A_1), the streamtube which is part of the control volume for determining gross thrust (A_2), and the part of the ducting channel that is outside the stream tube (A_4). The exit drag, D_e, is the force acting on the nozzle exit area (A_4). In the following, only pressure forces will be considered, since the contributions from friction are very small.

5.2.1 Intake Drag

The intake drag is caused by the forces acting on surfaces A_1, A_2 and A_4 (Figure 12) and is defined as follows,

$$D_i = -\iint_{A_1+A_2} \sigma_x dA + \iint_{A_4} \sigma_x dA. \qquad (9)$$

The method for computing A_1, A_2 and A_4 is presented in (Eslamdoost 2014). The computed intake drag value at Froude number 0.8 is $+5.63\ N$. The forces acting on these surfaces are split into hydrostatic and the hydrodynamic components to track the source of the drag more in detail. The hydrostatic and hydrodynamic pressure distributions on A_1, A_2 and A_4 at $Fn = 0.8$ are shown in Figure 13 and Figure 14, respectively. Contributions to D_i from A_1, A_2 and A_4 at this Froude number are shown in Figure 15. Note that a positive contribution is obtained for a force in the negative x-direction for A_1 and A_2, but in the positive direction for A_4. The hydrostatic pressure force component is larger than the hydrodynamic force exerted on these surfaces. Since the projected area of A_1 and A_2 on the yz-plane is much larger than that of A_4, these two surfaces have the largest hydrostatic pressure force components but since the normal vectors to these surfaces have their longitudinal components in opposite directions, these two large hydrostatic force components have different signs and cancel each other to a large extent.

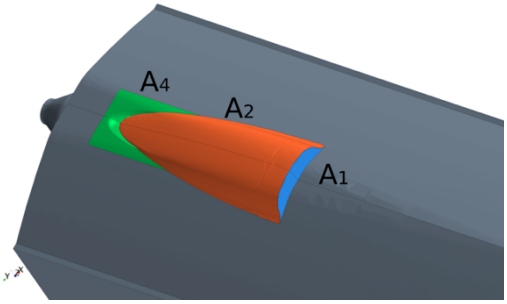

Figure 12 Computed A_1, A_2 and A_4.

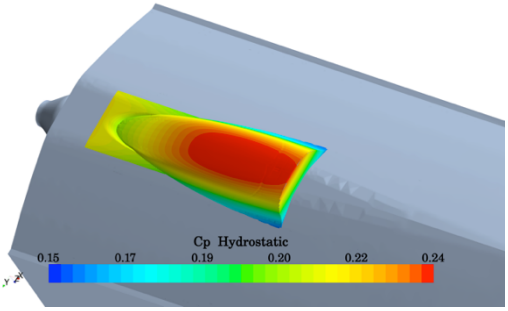

Figure 13 Hydrostatic pressure coefficient on A_1, A_2 and A_4 at Froude number 0.8 (bottom view)

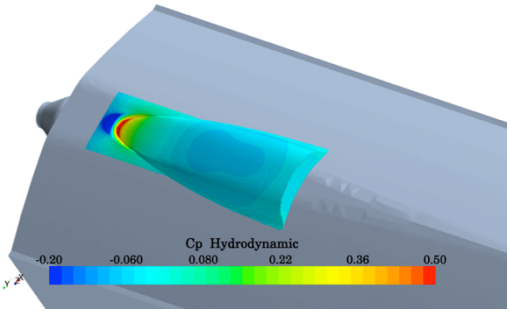

Figure 14 Hydrodynamic pressure coefficient on A_1, A_2 and A_4 at Froude number 0.8 (bottom view)

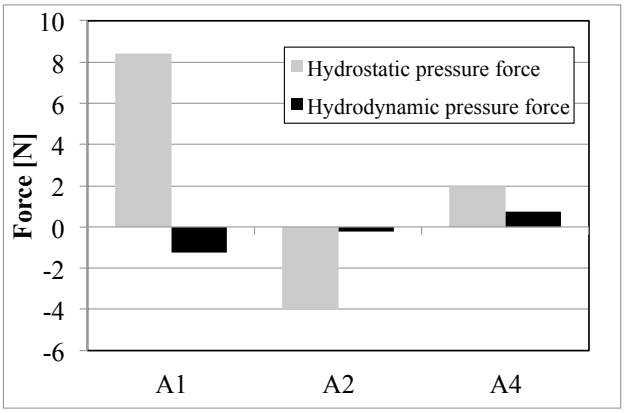

Figure 15 Hydrostatic and hydrodynamic pressure contributions to the intake drag

5.2.2 Exit Drag

The exit drag is caused by non-atmospheric pressure on the jet exit. In the literature (van Terwisga 1996; ITTC 2005) this component is assumed significant only if the exit is submerged. However, even if the jet is ejected into the air, the pressure will be non-atmospheric, unless the streamlines leaving the nozzle are exactly parallel. This is unlikely to be the case for most nozzles, and for the SSPA hull (Brown 2013) a relatively large pressure is found in the jet center. The pressure distribution is shown in **Figure 16**. Integrating this pressure over the nozzle exit area the exit drag is obtained. The computed exit drag at Froude number 0.8 is $-10.28\ N$.

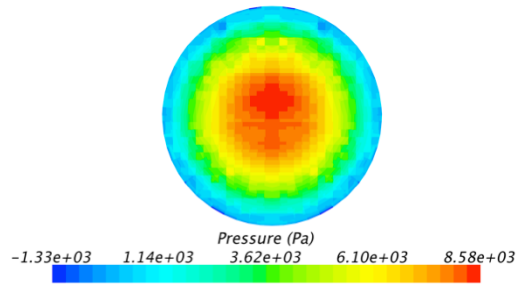

Figure 16 Total pressure distribution at the nozzle exit section at $Fn = 0.8$.

So far it has been assumed that the stator removes the entire swirl caused by the impeller, and therefore the jet is swirl free. However, in off design operating conditions of the waterjet pump the jet might not be entirely swirl free. The swirl at the nozzle exit results in a reduced pressure which changes the exit drag. There might also be an effect on the flow rate and consequently the gross thrust of the waterjet system. The effect of swirl is discussed at the end of this section.

5.3 Relative Importance of Intake and Exit Drag

As shown earlier the intake and exit drag at Froude number 0.8 are $+5.66$ and $-10.28\ N$, respectively. The sign of the intake drag and exit drag are opposite and the exit drag magnitude is larger than the magnitude of the intake drag, so the largest contribution to the difference between the gross and net thrust is the exit drag.

Using the computed values of the intake and the exit drag the jet thrust deduction fraction can be obtained using the following equation (Eslamdoost 2014),

$$t_j = \frac{D_i + D_e}{T_g}. \tag{10}$$

The computed jet thrust deduction fraction is -0.05. It should be noted that the jet thrust deduction fraction computed from the sum of the intake and exit drag, will not exactly cover the gap between the gross and the net thrust (as it should, since the last term of Equation (6) can be neglected for small t_r and t_j). The reason is that this gap is obtained as a small difference between two large numbers. The sum of the intake and exit drag, as computed here, should be more accurate.

6 CONCLUSIONS AND FUTURE WORK

There is just a minor change in the resistance of the self-propelled hull (net thrust) compared to the bare hull resistance ($t_r \approx 0$), and therefore the resistance increment cannot be considered as the main source of the observed negative thrust deduction fraction. Instead it is shown that the gross thrust is considerably smaller than the net thrust ($t_j < 0$) mainly due to the non-atmospheric pressure on the nozzle exit. This is the reason for the negative thrust deduction.

ACKNOWLEDGMENTS

The research presented has been sponsored by Rolls-Royce Marine through the University Technology Centre at Chalmers. Computing resources were provided by C3SE, Chalmers Centre for Computational Science and Engineering.

REFERENCES

Brown, Matz. 2013. “Model Tests of a Complete Waterjet-Hull System.” In . SSPA report RE40084817-16-00-B.

Bulten, Norbert Willem Herman. 2006. “Numerical Analysis of a Waterjet Propulsion System.” PhD Thesis, Eindhoven University of Technology.

Eça, Luis, and Martin Hoekstra. 2014. “A Procedure for the Estimation of the Numerical Uncertainty of CFD Calculations Based on Grid Refinement Studies.” *Journal of Computational Physics* 262: 104–130.

Eslamdoost, Arash. 2014. “The Hydrodynamics of Waterjet/Hull Interaction.” PhD Thesis, Shipping and Marine Technology, Chalmers University of Technology.

Eslamdoost, Arash, Lars Larsson, and Rickard Bensow. 2014a. "Waterjet Propulsion and Thrust Deduction." *Journal of Ship Research* 58 (4): 1–15.

Eslamdoost, Arash, Lars Larsson, and Rickard Bensow. 2014b. "On Transom Clearance." *Submitted to Ocean Engineering*.

ITTC. 1987. "Report of the High-Speed Marine Vehicle Committee." Kobe, Japan.

ITTC. 1996. "The Specialist Committee on Waterjets: Final Report and Recommendations to the 21st ITTC."

ITTC. 2005. "The Specialist Committee on Validation of Waterjet Test Procedures, Final Report and Recommendations to the 24th ITTC."

Van Terwisga, Tom. 1996. "Waterjet-Hull Interaction." PhD Thesis, Delft Technical University.

DISCUSSION

Question from Stefano Brizzolara

Your conclusion about t_r cannot be general as it is related to this particular case and Froude number. We found the opposite, in fact, especially in case of planning hulls. Can you comment on this?

Authors' Closure

The resistance increment fraction, t_r, of conventional designs of waterjet craft varies a lot at different speeds (see Eslamdoost, 2014). It has large positive values in the lower speed range (e.g. Fn<0.5) and then suddenly drops to values around zero in the intermediate speed range (e.g. 0.5<Fn<1) and eventually increases to moderately positive values in the high speed range (e.g. 1<Fn). In this paper, we have just studied the intermediate speed range where t is negative and t_r is close to zero. All the conclusions are just valid for this speed range and for the presented hull. Since t_r is a function of the bare hull and the waterjet driven hull resistance, it can even attain positive (but still close to zero) values in the intermediate speed range for the studied hull just by changing the LCG of the hull which means that the waterjet induced effects have increased the self-propelled hull resistance. However, if the LCG position variation stays within the conventional range, we should not expect large positive t_r values as reported for the lower speed range.

Question from Stefano Brizzolara

How do you account for the scale effects on the local flow corrections?

Authors' Closure

The scale effects cannot be neglected (especially, as stated in this question, the effects on the local flow). Different scaling methods have large impact on the thrust deduction fraction value. But since this study is carried out at model scale the scale effects are not considered.

Question from Neil Bose

The varied form of the thrust deduction with Froude number is a result of the definition of thrust deduction fraction as the difference between bare hull resistance and gross thrust. Is there an argument to be made for measuring the resistance of the self-propelled hull rather than the bare hull by using the plot of towing force versus thrust to get resistance and thrust deduction fraction?

Authors' Closure

It is feasible to measure the gross thrust, T_g, of a waterjet unit but unfortunately not its net thrust, T_{net}. If we had T_{net}, we could obtain the self-propelled hull resistance by subtracting the rope force from T_{net} (as proposed in the comment). But the gross and net thrusts are not the same and as indicated in Equation (8), the difference between them is equal to the sum of the Intake and Exit drags. These drag forces can be obtained through CFD simulation and not from measurement. It should also be mentioned that if in the future the CFD results become reliable enough, there will be no need for the calculation of the bare hull resistance and the thrust deduction fraction since the resistance of the waterjet driven hull and the required power can be computed directly from the self-propulsion simulation.